Carbohydrate Polymers 118 (2015) 224–234

Contents lists available at ScienceDirect

Carbohydrate Polymers

journal homepage: www.elsevier.com/locate/carbpol

Molecular, mesoscopic and microscopic structure evolution during amylase digestion of extruded maize and high amylose maize starches

Ashok K. Shrestha[a,c,d], Jaroslav Blazek[b,c], Bernadine M. Flanagan[a], Sushil Dhital[a], Oscar Larroque[c], Matthew K. Morell[c], Elliot P. Gilbert[b], Michael J. Gidley[a,*]

[a] Centre for Nutrition and Food Sciences, ARC Centre of Excellence in Plant Cell Walls, The University of Queensland, St. Lucia, Brisbane, Qld 4072, Australia
[b] Bragg Institute, Australian Nuclear Science and Technology Organisation, Locked Bag 2001, Kirrawee DSC, NSW 2232, Australia
[c] Commonwealth Scientific and Industrial Research Organisation, Food Futures National Research Flagship, Riverside Corporate Park, North Ryde, NSW, Australia
[d] School of Science and Health, The University of Western Sydney, Richmond, NSW, Australia

ARTICLE INFO

Article history:
Received 12 August 2014
Received in revised form 4 November 2014
Accepted 5 November 2014
Available online 20 November 2014

Keywords:
Extrusion
Starch structure
Maize
Amylose
Digestibility
Chain length

ABSTRACT

Extrusion processing of cereal starch granules with high (>50%) amylose content is a promising approach to create nutritionally desirable resistant starch, i.e. starch that escapes digestion in the small intestine. Whilst high amylose content seems to be required, the structural features responsible for the slow digestion of extrudates are not fully understood. We report the effects of partial enzyme digestion of extruded maize starches on amylopectin branch length profiles, double and single helix contents, crystallinity and lamellar periodicity. Comparing results for three extruded maize starches (27, 57, and 84% apparent amylose) that differ in amylase-sensitivity allows conclusions to be drawn concerning the rate-determining features operating under the digestion conditions used. Enzyme resistance is shown to originate from a combination of molecular and mesoscopic factors, including both recrystallization and an increase in very short branches during the digestion process. This is in contrast to the behaviour of the same starches in the granular form (Shrestha et al., 2012) where molecular and mesoscopic factors are secondary to microscopic structures in determining enzyme susceptibility. Based on the structure of residual material after long-time digestion (>8 h), a model for resistant starch from processed high amylose maize starches is proposed based on a fringed micelle structure with lateral aggregation and enzyme susceptibility both limited by attached clusters of branch points.

1. Introduction

The nutritional properties of starches depend on both their botanical origin and the nature of any food processing operations, and are largely determined by the rate of digestion. Fast digestion by (initially) α-amylase typically results in the rapid uptake of glucose, the secretion of insulin to manage the absorbed glucose and a consequent hypoglycaemic overshoot, a series of events which if repeated often enough, is considered a risk factor for diabetes (Howlett & Ashwell, 2008). Digestion which is sufficiently slow results in (a portion of) starch escaping digestion in the small intestine and therefore entering the large intestine where it is fermented by bacteria producing primarily acetate, propionate and butyrate end products instead of glucose. This so-called resistant starch (Bird, Lopez-Rubio, Shrestha, & Gidley, 2009; Topping & Clifton, 2001) in stark contrast to fast digested starch, is considered to have high nutritional value not only by promoting beneficial microflora and colonic health but also through reducing energy intake and prolonging satiety. Thus the rate and/or extent of enzymic digestion of starch in the small intestine has the potential to be the difference between a high nutritional value dietary component and one that is a disease risk factor.

Starches contain two limiting types of α-(1–4)-linked glucose polymers, the largely linear amylose and the highly branched amylopectin. High (>50%) amylose starches have repeatedly been shown to have amylase digestion rates slow enough to result in nutritionally significant amounts (more than 10% and often much higher) surviving to the large intestine with consequent health benefits (Bird, Vuaran, & Topping, 2007; Zhang & Hamakar, 2010). As starches are typically the major energy source in a diet, high levels of resistant starch have a major potential consequence for human health, and understanding the mechanism(s) underlying slow digestion rates provides an opportunity to optimize nutritional value.

* Corresponding author. Tel.: +61 7 3365 2145; fax: +61 7 3365 1177.
E-mail address: m.gidley@uq.edu.au (M.J. Gidley).

http://dx.doi.org/10.1016/j.carbpol.2014.11.025
0144-8617/

General mechanisms leading to slow digestion and resistant starch formation have been identified (Dhital, Warren, Butterworth, Ellis, & Gidley, 2015) based on (a) barriers that slow down or prevent access/binding of enzyme to starch; and (b) starch structural features that slow down or prevent amylase action when access is not limiting. Starch-containing structures which contain these features have been categorized as (1) physically inaccessible starch, (2) certain ungelatinised granules, (3) cooked and aged ('retrograded') processed starches, (4) chemically modified starches, and (5) lipid-complexed starches (Bird et al., 2009). Whereas types 1, 4, and 5 mostly rely on non-starch components to slow down digestion, types 2 and 3 rely on intrinsic structural features of starches. As most starch in the human diet is cooked before consumption, understanding the mechanism(s) underlying the slow digestion of cooked and aged starches is important in order to provide design rules for food processing with beneficial nutritional outcomes.

Most previous studies of the digestion of cooked and aged starches have characterized structural features prior to digestion (Cairns, Sun, Morris, & Ring, 1995; Gidley et al., 1995; Sievert & Pomeranz, 1989), and have emphasized the re-crystallization processes that can occur after starch is cooked and cooled/aged (Chanvrier et al., 2007; Doutch et al., 2012; Eerlingen, Crombez, & Delcour, 1993; Eerlingen, Deceunick, & Delcour, 1993; Gidley et al., 1995; Shrestha et al., 2010; Siljestrom, Eliason, & Bijorck, 1989). The fact that amylose re-crystallizes faster and to a more stable crystalline form than amylopectin (Planchot, Colonna, & Buleon, 1997; Williamson et al., 1992) is consistent with the general finding of slow digestion rates for cooked and cooled/aged high amylose starches (Clarke, Bird, Topping, & Cobiac, 2007; Shrestha et al., 2010). However, high temperature/pressure processing of high amylose starches followed by rapid drying such as in extrusion can generate materials that are only weakly crystalline yet still very slowly digested (Htoon et al., 2009; Shrestha et al., 2010; Sievert, Czuchajowska, & Pomeranz, 1991). One possible reason for this is that crystallinity is recovered during the enzyme digestion process. Evidence for this has been obtained from X-ray scattering studies of extruded and partly digested high amylose starches (Lopez-Rubio, Flanagan, Shrestha, Gidley, and Gilbert, 2008). However, there has been no detailed study to date of the parallel evolution of molecular structure and indices of higher order structures linked with digestion rates. The aim of this work is therefore to compare the molecular (<10 nm), mesoscopic (10–100 nm) and microscopic (>100 nm) structures of partially digested extruded maize starches varying in amylose content (27%, 57%, 84%) and digestion rate. Examination of samples by a wide range of techniques (fluorophore-assisted capillary electrophoresis, X-ray scattering and diffraction, NMR spectroscopy and scanning electron microscopy) allows a coherent framework to be developed. This is contrasted with data from a similar study of the same starches in uncooked granular form (Shrestha et al., 2012) to show that there are qualitatively different mechanisms responsible for slow digestion of granular and extruded starches.

2. Experimental

2.1. Materials

Two high amylose maize starches (HAMS), Gelose 50 (G50) and Gelose 80 (G80), and a regular maize starch (RMS) were purchased from Penford Australia Ltd, Lane Cove, Sydney, Australia. The apparent amylose contents of RMS, Gelose 50 and Gelose 80 were found to be 27.1, 57.5, and 83.6% respectively using an iodine colorimetric method as described previously (Htoon et al., 2009).

The following enzymes and chemicals were obtained from local distributors: α-amylase (Sigma A-3176 Type VI-B from porcine pancreas), pepsin (Sigma P-6887), pancreatin (Sigma P-1750 from porcine pancreas), amyloglucosidase (Sigma A-7420 from *Aspergillus niger*), RMS (Sigma S-5296), α-amylase (3000 U/mL, Megazyme E-BLAAM from *Bacillus licheniformis*), amyloglucosidase (3200 U/mL, Megazyme E-AMGDF), enzyme glucose reagent (glucose oxidase/peroxidase; TR15104, Thermoelectron), isoamylase from *Pseudomonas* sp. (250 Unit/mL, Megazyme), APTS or 8-amino-1,3,6-pyrene trisulfonic acid (Sigma), Wizard mini column (Promega, Australia), pullulan (P-82, Lot 80101, Shodex) and poly (ethylene oxide) standards (WAT 035711) (from Polymer Standard Service, RI, USA). Freshly prepared distilled de-ionized water was used for reagent preparation as well as for sample analysis.

2.2. Extrusion

Extrusion was carried out in a Prism Eurolab^{TM} co-rotating twin screw extruder (Thermo Prism, Staffordshire, UK), with a screw diameter of 16 mm and an extruder barrel 640 mm long, giving a length to diameter (L/D) ratio of 40:1. Details of the extruder and extrusion conditions have been described previously (Shrestha et al., 2010). In this study, all other extrusion parameters, e.g., screw speed, temperature profile and feed rate were kept the same except for the liquid feed rate, which was used to vary the final moisture content. Based on the given data, the total specific mechanical energy (SME) input during extrusion was estimated using Eq. (1) (Bhattacharya and Chaudhury, 1994).

$$\mathrm{SME} = \frac{\mathrm{RPM\ of\ screw\ (run)}}{\mathrm{RPM\ of\ screw\ (rated)}} \times \frac{\%\mathrm{Torque}}{100} \times \frac{\mathrm{Motor\ power\ (rated)}}{\mathrm{Production\ capacity}} \quad (1)$$

The extruder was run at the required set of barrel temperatures, screw speed, Auger speed and high (>7 g/min) liquid feed rate for about 15 min. Once the system was stable, the liquid feed rate was set at the level needed to achieve moisture contents of 30%, 45%, or 60% within the extruder. Extrusion was carried out for 15–20 min before samples were collected to ensure steady state conditions. The moisture content of extrudates was immediately measured by a previously calibrated infrared moisture metre (Sartorius Moisture Analyzer, NY). Extrudates were cut into approximately 12 cm lengths, cooled to room temperature, packed in Cryovac bags, and stored for 0 (fresh) or 12 days (stored) at 4 °C. The extrudates were freeze dried and then cryo-milled for 10 min into fine powders (Freezer/Mill, Metuchen, NJ, USA). The cryo-milled extrudates from all three starches were sieved and particles (sizes 180–600 μm) were transferred into small plastic containers, tightly capped, and stored at room temperature until further use. This relatively narrow range of particle size of extrudates was used as our previous study showed that the digestibility of the extrudates was affected by the particle size (Shrestha et al., 2010).

2.3. Enzyme digestion

The in vitro enzyme digestion of maize extrudates followed the method described previously (Htoon et al., 2009) with slight modification. In brief, the method involved initial treatment of starch with artificial saliva (α-amylase in carbonate buffer) followed by acidification and digestion with pepsin. The neutralized starch mass was further incubated with pancreatin and amyloglucosidase at pH 6.0 for 0.0, 0.5, 1.5, 4.0, 8.0, and 24 h. Digested starch mass was immediately transferred to a boiling water bath for 2 min, cooled, centrifuged and the supernatant was analyzed for glucose content using enzyme glucose reagent. A digestogram was established by plotting glucose release as a function of incubation time.

The undigested residue left after centrifugation was freeze-dried, weighed and divided by original weight to calculate % yield.

2.4. X-ray diffraction (XRD)

XRD measurements of samples were made with a Panalytical X'Pert Pro diffractometer. The instrument was equipped with a copper X-ray generator ($\lambda = 1.54$ Å), programmable incident beam divergence slit and diffracted beam scatter slit, and an X'celerator high speed detector. X-ray diffraction patterns were acquired at room temperature over the 2θ range of 2° to 40° with a step size of 0.0330° 2θ and a count time of 400 s per step.

Assuming a constant divergent slit and a flat-surfaced sample of semi-infinite depth during XRD measurement, the experimentally-obtained diffraction patterns were decomposed into a series of discrete diffraction peaks (corresponding to the crystalline phase) and two or three broad peaks (corresponding to the amorphous phase) using the modified curve-fitting procedure of Lopez-Rubio, Flanagan, Gilbert, and Gidley (2008). Crystallinity was calculated as the percentage proportion of the area under the crystalline peaks (A or B type) to the total area, which was calculated as the area between the experimental data and the baseline. The baseline was determined by collecting a diffraction pattern from an empty sample holder corresponding to the scattering from the instrument and air. The proportion of V-type crystallinity was determined as the area under the crystalline peaks at 7, 13 and 20° 2θ divided by the total minus the baseline area.

2.5. Small angle X-ray scattering (SAXS)

SAXS measurements were obtained made using a Bruker NanoStar SAXS instrument equipped with a Vantec 2000 area detector (effective pixel size 54 μm) and pin-hole collimation for point focus geometry. The X-ray source was a copper rotating anode (0.3 mm filament) operating at 45 kV and 110 mA, fitted with cross coupled Göbel mirrors, resulting in a Cu K_α radiation wavelength of 1.5418 Å. The optics and sample chamber were under vacuum to minimize air scattering. The sample to detector distance was chosen to be 700 mm, which provided a q-range from 0.014 to 0.430 $Å^{-1}$. Samples were presented in 2 mm sealed quartz capillaries as suspensions containing excess water above the sedimented sample and scattering was measured for 60 min. Scattering data were background corrected based on the scattering from the capillary filled with water. SAXS datasets were radially averaged using Bruker AXS software 4.1.30. SAXS curves were normalized to sample transmission and background-subtracted using Igor software (Wavemetrics, Lake Oswego, Oregon, USA).

2.6. Solid state ^{13}C nuclear magnetic resonance (NMR) spectroscopy

Solid starch samples were analyzed by ^{13}C NMR spectroscopy before and after enzyme digestion using the spectral acquisition and interpretation methodology described in Tan, Flanagan, Halley, Whittaker, and Gidley (2007). The solid-state ^{13}C CP/MAS NMR experiments were performed at a ^{13}C frequency of 75.46 MHz on a Bruker MSL-300 spectrometer. Approximately 200–300 mg of starch was packed in a 4-mm diameter, cylindrical, PSZ (partially stabilized zirconium oxide) rotor with a perfluorinated polymer (KelF) end cap. The rotor was spun at 5–6 kHz at the magic angle (54.78°). The 90° pulse width was 5 μs and a contact time of 1 ms was used for all starches with a recycle delay of 3 s. The spectral width was 38 kHz, acquisition time 50 ms, time domain points 2000, transform size 4000, and line broadening 50 Hz. At least 2400 scans were accumulated for each spectrum. Spectra were referenced to external adamantine. The analysis of the NMR spectra involves the decomposition of the spectrum into amorphous and ordered sub-spectra as explained elsewhere (Tan et al., 2007) This provides a quantitative analysis of double helices, single helices, and amorphous conformational features within solid starch samples. The method gives accurate (±2%) quantification of double helix and single helix contents, but accuracy is reduced for samples with very low (<10%) total helix content as the method involves the subtraction of amorphous spectral signals from the sample spectrum, so a low helix content results in almost complete subtraction of signals, with resulting uncertainty in the residual double/single helix signal intensity.

2.7. Scanning electron microscopy (SEM)

For SEM, dried extruded and residues from digested starch powders were thinly spread on to circular metal stubs coated with double-sided adhesive carbon tape. The stubs were transferred to a desiccator containing P_2O_5, placed under vacuum and left overnight at room temperature. The powder on the stubs was platinum coated using an Eiko IB-5 Sputter Coater (at 6 mA, 5 min. for medium coating) in an argon gas environment, yielding approximately 15 nm coating thickness. The coated samples were imaged in a JEOL 6400 JSM Scanning electron microscope (JEOL Ltd., Tokyo, Japan). The accelerating voltage used was 10 kV and the working distance was set at 15 mm. Representative micrographs were taken at low magnification followed by higher magnification up to 20,000 times.

2.8. Fluorophore assisted carbohydrate electrophoresis

The debranched and fluorescence labelled starch samples were prepared as described by Castro, Ward, Gilbert, and Fitzgerald (2005), with slight modification. About 20 mg of accurately weighed extrudate or enzyme-digested starch residues in a 2 mL Eppendorf tube (in duplicate) were dispersed with water (750 μL). The dispersion was mixed with 2 M NaOH (50 μL), placed in a boiling water bath for 5 min and cooled to room temperature. The gelatinized mass was acidified with glacial acetic acid (32 μL) and buffered with 1 M sodium acetate (100 μL). The mixture was diluted with water (1 mL) followed by isoamylase (10 μL) and mixed. The isoamylase digestion of starches produces a population of linear oligosaccharides with degree of polymerization between three and 85 which can be resolved by capillary electrophoresis (Morell, & Samuel, O'Shea, 1998; Shea, Samuel, Konic, & Morell, 1998). The tube was incubated at 37 °C for 2 h and enzyme deactivated by boiling for 10 min. An aliquot (50 μL) of debranched starch was transferred to a small glass bottle and freeze dried. The released oligosaccharides were fluorescence labelled by incubating overnight at 37 °C with 3.5 μL of APTS (8-amino-1,3,6-pyrenetrisulfonic acid) solution (5 mg APTS in 48 μL 15% acetic acid) and 3.5 μL of sodium cyanoborohydride (16 μL water per mg solid). The labelled sample was mixed with 6 M urea (40 μL) and water (40 μL) and boiled for 1 min. Finally, the mixture was filtered through a Wizard mini column into a fresh Eppendorf tube by spinning at 5000 × g in a microcentrifuge for 2 min. Capillary electrophoresis of APTS labelled oligosaccharides to determine the branch length profile (O'Shea et al., 1998) was performed on a P/ACE 5010 capillary electrophoresis system (Beckman Coulter, Gladesville, NSW, Australia) with argon-LIF detection. Results are plotted as a normalized signal representing the percentage of the total analyzed chain population found for each discrete chain length. The longer chain lengths in the samples (>DP 80), e.g., amylose chains, cannot be detected by this system, thus this analysis of the debranched starch is principally an analysis of debranched amylopectin (Morell et al., 1998).

3. Results

3.1. Extrusion and enzyme digestion rates

Table 1 shows the extent of starch digestion after defined incubation times in granular (raw) and extruded starches, and illustrates how both amylose content and extrusion conditions affect digestion extents. The percentage in the sample name refers to the final moisture content after extrusion. Compared to the relevant granular starch, digestion was much higher in the extruded form, as reported in our previous paper (Shrestha et al., 2010). Granular regular maize starch is inherently digestible due to its low amylose content, abundant surface pores, and voids within the granule interior (Blazek & Gilbert, 2010; Dhital, Shrestha, & Gidley, 2010; Shrestha et al., 2010), and even more digestible after extrusion with almost 50% of extruded starch digested within 30 min of digestion. Higher amylose starches which are similarly resistant to digestion in the granular form (29.0 and 26.6% digested after 24 h) are also similarly resistant after extrusion although much less so than the granule form with about 15% digested within 30 min, ~50% in 4 h and ~80% after 24 h. Various factors leading to the lowering of enzyme resistance of starch during extrusion cooking have been reported in our previous studies (Htoon et al., 2009; Lopez-Rubio, Flanagan, Shrestha et al., 2008; Shrestha et al., 2010).

All the starches were extruded with liquid feed rates calculated to achieve moisture contents of 30, 45, and 60% (dry basis), but lower water contents were found in the extrudates (Table 1), most probably due to loss of water during expansion (pressure drop) while exiting from the die. Although three liquid feed rates were set to achieve extrudates with three different moisture levels, for RMS, feed rates set to achieve 45 and 60% moisture both resulted in extrudates with 40% moisture, therefore, only two extruded RMS samples with final moisture levels (29 and 40%) could be achieved. The product yield rates were higher for RMS compared to HAMS which could be due to their greater tendency to gelatinize under the extrusion conditions (<120 °C). HAMS may not undergo complete gelatinization, due to their relatively extended phase transition, from ~70 to 120 °C in the presence of excess water (results not shown), and the presence of limiting water during extrusion which will further raise the phase transition temperature. SME values for extrusion of HAMS were higher than for RMS as more energy is needed to de-structure the more thermally stable crystallites in HAMS compared with RMS. Wang et al. (2010) also reported that whereas HAMS are rigid and resistant to shear force, regular maize starch could easily undergo structural changes under shear treatment which affects the energy input during extrusion. Extrusion data (Table 1) also showed that a higher torque (and SME) is required to gelatinize/melt starches for lower water contents. Water acts as a plasticizer of the molten starch mass inside the barrel that lowers the torque needed to mix and propel the viscous mass. At similar moisture content (~30%), the torque values for RMS, G50 and G80 were 6.2, 7.0 and 7.4 N.m (data not shown), a trend also observed by Wang et al. (2010) in similar starches. This indicates that maize starches with high amylose also need higher torque to destroy the granule structure compared to more amylopectin-rich starch granules.

In extrusion processing, expansion of extrudate occurs as the water under high pressure is suddenly released while exiting from the die orifice. The swelling/expansion ratios of RMS extrudates were much higher than those for HAMS (Table 1). High amylopectin starches tend to absorb more water, and undergo swelling and disintegration at about 80 °C. Water absorption and swelling behaviour of HAMS is, however, strongly inhibited by its high amylose content as well as lipid (as amylose–lipid complex) because of the consequent elevated temperature (>90 °C) and greater water contents required to cause crystallite dissociation and swelling. The current extrusion processing was carried out at 120 °C, with a low torque and relatively low amount of water (20–60%), a condition leading to only partial hydration of HAMS due to incomplete gelatinization/cooking (as judged by residual helix content and crystallinity – see Section 3.3) which may have contributed to the lower expansion ratios of extrudates.

Native starch granules from various sources such as potato and banana have high resistant starch contents, but once processed, these starches are almost completely digestible (Bello-Perez, Ottenhof, Agama-Acevedo, & Farhat, 2005; Kingman & Englyst, 1994). In contrast, extruded high amylose starches still retained significant levels of enzyme resistance. Table 1 shows that a significant amount of starch from extruded HAMS resisted digestion even after 24 h, up to 22.5% and 30.4% for G50 and G80, respectively. This is a large amount of enzyme resistant starch from a single source that can be potentially used in food formulations to increase the resistant starch content of extruded foods. The relative in vitro enzyme digestibility of the extruded samples is consistent with the reduced glycemic response and increased resistant starch levels found for processed high amylose cereals (Bird et al., 2009).

Despite being processed under the same operating conditions, moisture addition and feed rates, final extrudate moisture contents and expansion ratios varied with starch type (Table 1). This variation is indicative of materials/machine interactions caused by the different rheology of each of the starches, and is also reflected in the extent of structure loss. However, as the purpose of this study is to characterize the general pattern of enzyme digestion of extruded starches, modest differences in extrudate properties

Table 1
Extrusion parameters and digestibility of extruded starches after defined enzyme digestion times.[a]

Samples	Product yield (g/min)[b]	SME[c] (kJ/kg)	Expansion ratio[d]	Incubation times (h) and % Digestibility				
				0.5	1.5	4.0	8.0	24.0
RMS, Raw	–	–	–	18.8	47.8	78.8	87.5	99.5
RMS, 29.0%	9.8	159	1.69	47.9	63.6	89.9	96.6	100.0
RMS, 40.0%	12.2	85	1.50	56.1	75.2	92.4	94.6	94.4
G50, Raw	–	–	–	5.5	10.0	16.6	21.3	29.0
G50, 24.0%	8.4	230	1.05	16.5	35.5	47.8	65.0	81.6
G50, 30.7%	7.0	165	1.09	14.4	27.9	54.8	67.5	83.2
G50, 35.1%	4.8	113	1.11	16.5	27.2	46.9	64.9	77.5
G80, Raw	–	–	–	4.6	8.1	13.5	19.1	26.6
G80, 20.8%	10.1	315	1.00	26.8	33.6	61.4	77.0	86.5
G80, 30.4%	7.4	232	1.11	16.4	35.8	52.0	65.1	73.8
G80, 36.3%	6.2	195	1.04	15.5	22.0	42.4	53.1	69.6

[a] Values given against various starches are moisture content of extruded starches.
[b] Product yield is calculated by weighing starch extrudate yield from extruder in a given time.
[c] Specific mechanical energy.
[d] Diameter of extrudate divided by diameter of the orifice.

Table 2
Chain length distribution of debranched extruded and digested starches.

Starches and digestion times (h)	%Amylopectin chain lengths, degree of polymerization			
	<13 DP	13–24 DP	25–36 DP	>36 DP
Regular maize starch				
Raw	32.7	52.2	9.1	6.0
Extrudate, 29.0%MC	36.9	53.6	7.6	1.7
Extrudate, 40.0%MC[a]	37.2	53.0	8.0	1.8
Ex RMS 0.5 h	35.7	53.1	8.7	2.5
Ex RMS 1.5 h	35.2	53.9	8.6	2.3
Ex RMS 4.0 h	34.7	53.9	8.9	2.5
Ex RMS 8.0 h	34.4	54.2	9.0	2.3
Ex RMS 24.0 h	34.2	53.2	9.1	3.4
Gelose 50				
Raw	21.5	51.4	14.0	12.8
Extrudate, 30.7%MC	28.7	58.2	10.6	2.5
Extrudate, 35.%MC	30.4	59.1	8.8	1.2
Extrudate, 24.0%MC[a]	25.7	58.7	11.8	3.5
Ex G50 0.5 h	25.8	57.9	12.1	3.7
Ex G50 1.5 h	25.8	54.3	13.2	5.5
Ex G50 4.0 h	21.7	58.7	14.8	4.6
Ex G50 8.0 h	29.3	54.7	12.1	3.6
Ex G50 24.0 h	37.3	48.1	10.4	3.3
Gelose 80				
Raw	21.7	51.4	14.0	13.1
Extrudate, 30.4%MC	24.4	58.6	13.1	3.9
Extrudate, 36.3%MC	28.8	56.6	11.6	2.0
Extrudate, 20.8%MC[a]	25.0	57.4	13.9	3.3
Ex G50 0.5 h	25.3	57.4	13.6	3.5
Ex G50 1.5 h	26.2	57.2	13.4	2.9
Ex G50 4.0 h	29.6	54.2	12.8	2.8
Ex G50 8.0 h	31.4	49.5	13.5	4.8
Ex G50 24.0 h	38.6	42.9	12.6	4.5

[a] Extruded starches, each of which are enzymatically hydrolysed from 0.5 to 24 h.

between samples are not critical. In addition, subsequent structural analyses confirmed that molecular, crystalline and microscopic structures had been modified to a similar extent in each sample, thus further suggesting that comparative analyses are meaningful.

3.2. Branch length profiles of high amylose extrudates are affected by digestion

Extrusion is expected to cause molecular degradation of starches. Of particular interest in this study was the unit chain length profile of the debranched starch, as it is the branched amylopectin fraction that is primarily responsible for the crystallinity of starch granules and which is expected to be disrupted during extrusion. Interestingly, there was very little difference in chain length distribution of granular RMS and both extruded starches across all the chain length distribution (Table 2, Fig. 1), except for DP > 36 that showed a reduction from 6 to ~1.7% DP. Table 2 shows an increase in relative abundance in chain lengths of <13 DP and 13–24 DP for all extrudates, balanced by a decrease in longer chains of 25–36 DP and >36 DP, e.g., from 12.8 to 1.2% or 10 times decrease in long chains (>36 DP) in G50. The striking decrease in relative abundance of chains longer than 36 units suggests that extrusion processing specifically cleaves chains that link adjacent amylopectin clusters (termed B2 and B3 in Hizukuri (1986)). As there are considered to be relatively few chains linking amylopectin clusters, these chains carry a high mechanical strain that might be expected to make them vulnerable to scission during high energy extrusion processing, particularly under conditions where there is residual granular structure. It is of interest that similar changes are also seen on initial enzyme digestion of unprocessed granules (Shrestha et al., 2012), suggesting that in general inter-cluster chains are the most susceptible to cleavage by either mechanical or enzymic means.

FACE data for RMS showed that the amylopectin branches resisting digestion show remarkably little difference up to 24 h digestion (after which almost 95% starch had been digested), similar to findings for granular versions of all three maize starches, where branch length distributions showed only minor changes during the course of digestion (Shrestha et al., 2012) (Fig. 1). This is consistent with the rate limiting step for enzyme digestion of extruded maize starch being binding rather than catalysis (Dhital et al., 2015), i.e. if enzyme binding to a region of extruded starch is slower than the subsequent digestion of that region, then partially digested remnants from this region are unlikely to be recovered. Branch length profiles of residual undigested material after enzyme treatment are thus likely to be very similar to those of the starch prior to enzyme digestion, i.e. if digestion after binding is faster than (rate-limiting) enzyme binding then residual fragments are more likely to represent regions which have not had enzyme bound rather than regions which are in the process of being digested by bound enzyme. Size exclusion chromatography (SEC) of extruded RMS and waxy maize starch also showed both amylose and amylopectin levels decrease with time and that complete loss occurs within 2 h of digestion (Witt, Gidley, & Gilbert, 2010).

However, a different picture emerges for HAMS extrudates (Fig. 1). For G50 and particularly G80, enzyme resistant fractions contain an increased number of short branches (39% DP < 13 after 24 h digestion) compared with the starting extrudate (25%, Table 2). Whilst enzyme digestion of branches will inevitably produce a series of shorter branches as intermediate components (Fig. 1), it is not obvious why these should be enzyme resistant unless they are part of a highly branched local structure which provides a topological barrier to enzyme access. This latter mechanism can be inferred from studies of the rate of enzyme digestion of branched starch-based polymers which show that for very short average branch lengths, rates of amylolytic digestion decrease (Ao et al., 2007; Zhang, Zihua, & Hamaker, 2008). What is not clear from these data alone is why HAMS should show this effect but not RMS (Fig. 1). Our previous study showed that the digestion of extruded HAMS could lead to increased molecular order, most likely due to short amylose chains generated during the hydrolysis process which are able to re-associate, forming an enzyme resistant fraction (Lopez-Rubio, Flanagan, Gilbert et al., 2008). It seems unlikely, however, that short branch length amylopectin fragments which are not capable of crystallizing could be incorporated into a crystalline structure (Eerlingen, Crombez et al., 1993; Eerlingen, Deceunick et al., 1993; Gidley et al., 1995). However, if they were covalently attached to linear chain portions which are insoluble due to a high level of molecular order, this could explain why short branch glucans remain in the solid phase following enzyme digestion system.

3.3. Helix and crystallite formation during enzyme digestion

Extrusion processing of each starch resulted in a significant reduction in molecular order or helical content by NMR and crystallinity by XRD compared to the corresponding granular form (Table 3 and Fig. 2). The reduction in molecular order (sum of A/B and V types) from NMR was greater for RMS (total of A- and V-type of 12% cf 45%) than either of the HAMS (totals of B- and V-type 22% cf 35% for G50; 15% cf 27% for G80). This could reflect incomplete gelatinization of HAMS, but may also be due to recrystallization during extrusion processing. Support for the latter comes from the crystalline form for RMS which changes from A-type in the granular form to a mixture of A and B forms after extrusion (Fig. 2), with a greater relative amount of B-type (increased intensity at 17 cf 18° 2θ) at higher moisture. The similar levels of total crystallinity (sum of A/B and V types) for the three extruded samples (11.7% cf 12.9% cf 10.3%) is also consistent with all three starches

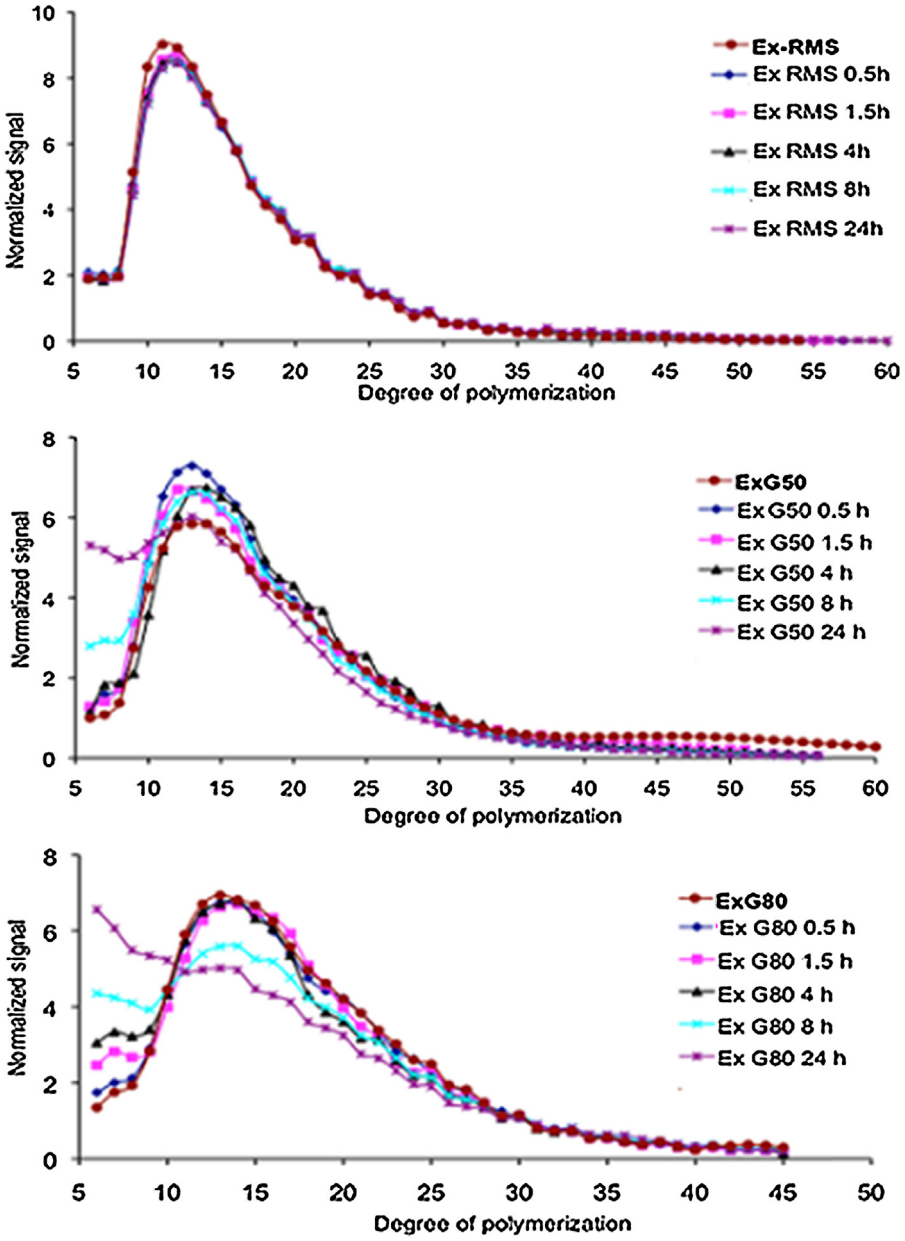

Fig. 1. Chain length distribution in debranched amylopectin of extruded regular maize starch (RMS), Gelose 50 (G50) and Gelose 80 (G80) before and after enzyme digestion for 0.5 h, 1.5 h, 4 h, 8 h, and 24 h.

having undergone recrystallization during the overall extrusion process.

Quantitative analysis of X-ray diffraction patterns and solid state NMR spectra demonstrated a clear increase in both molecular and crystalline order in material that remains undigested after increasing enzyme incubation times. The evolution of crystalline order in the extruded starches and the residues left after digestion is shown for G50 as a series of X-ray diffraction patterns in Fig. 2; similar patterns were seen for G80 (data not shown).

The greater values for NMR measures of molecular helix order than X-ray measures of crystalline order reflect the presence of some helices (both double helical A/B and single helical V types) that are not packed sufficiently regularly or extensively to form long-range crystalline order. This difference in X-ray and NMR measures of order is magnified greatly on prolonged digestion (>8 h) with 66 and 71% helical order (sum of A/B/V types) detected for 24 h undigested residues for G80 and G50 respectively, whereas the corresponding values for crystalline order (sum of A/B/V types) are 31 and 29% respectively (Table 3). Thus extensive resistance to enzyme digestion (after e.g. 24 h) is associated with a high level of double-helical (and to a lesser extent single helical) order, most of which is not present within crystallites. This behaviour is in stark contrast to the effect of enzyme digestion on the same starches in granular form where there were only slight increases in helical and crystalline order associated with enzyme-resistant residues (Shrestha et al., 2012). The extrusion process mobilizes polymer chains which are likely to be more able to subsequently rearrange to adopt ordered helical structures than the spatially constrained chains within (partly digested) granules.

An increase in the relative amount of molecular or crystalline order during digestion could be associated with either selective digestion of non-ordered material and/or retrogradation (recrystallization) during the digestion process. For RMS, a rise in A/B type X-ray crystallinity from 9.9% prior to digestion to 26.1% after 0.5 h

Table 3
Crystallinity and helical order (%) of extruded starches before and after amylase digestion calculated from NMR.

Starch types[1]	Type of helix/order (%)	Digestion times						
		Raw starch	Extruded starch[2]	0.5 h	1.5 h	4 h	8 h	24 h
Regular maize starch	Double helix, A-type %	33	11	NA	NA	NA	NA	NA
	Single helix, V-type, %	12	1	NA	NA	NA	x	NA
	Non-ordered, %	55	88	NA	NA	NA	NA	NA
	XRD A/B-type crystallinity, %	30.0	9.9	26.1	24.7	NA	NA	NA
	XRD V-type crystallinity, %	1.9	1.8	1.5	1.7	NA	NA	NA
Gelose 50	Double helix, B-type %	23	17	20	24	17	29	62
	Single helix, V-type, %	12	5	5	7	6	9	9
	Non-ordered, %	65	78	75	69	78	62	29
	XRD A/B-type crystallinity, %	27.4	11.1	13.5	14.2	13.4	NA	27.4
	XRD V-type crystallinity, %	2.1	1.8	2.5	2.2	1.7	NA	1.6
Gelose 80	Double helix, B-type %	21	12	26	28	40	39	57
	Single helix, V-type, %	6	3	5	6	8	8	9
	Non-ordered, %	73	85	69	66	52	53	34
	XRD A/B-type crystallinity, %	23.2	9.5	16.6	18.0	19.6	20.0	28.8
	XRD V-type crystallinity, %	2.1	0.8	2.4	2.0	1.9	2.0	2.0

NA, Data not available due to lack of enough samples.

results in 56.1% digestion (Table 1). If all of this digestion was of non-ordered material and there was no retrogradation, the crystallinity value should have been 22.6% (9.9/[100 − 56.1] × 100%). Thus there must have been at least some retrogradation during the first 0.5 h of digestion for extruded RMS. Similar considerations apply for the first 0.5 h digestion of G80 where double helix order increases from 12 to 26% whilst there is only 15.5% digestion. If all this digestion was of non-ordered material and there was no retrogradation, then the double helix order should have been 14.2%; this thus demonstrates that significant retrogradation has occurred. Interestingly, the same conclusions are not drawn for G50, where the steady rise in B-type crystallinity with digestion time is similar to that which is predicted for digestion of only non-ordered material. However, for G50, the major retrogradation event occurred between 8 h and 24 h where a more than doubling of the double helix content from 29% to 62% (Table 3) occurred alongside a much smaller difference in digestibility of 65–77% (Table 1).

3.4. Small angle X-ray scattering changes during digestion

Small angle X-ray scattering of extruded G50 and G80 samples are shown in Fig. 3) on logarithmic scales to highlight different regions of the scattering profiles. There is an absence of the q ca. 0.06–0.07 A^{-1} peak associated with the characteristic 9–10 nm

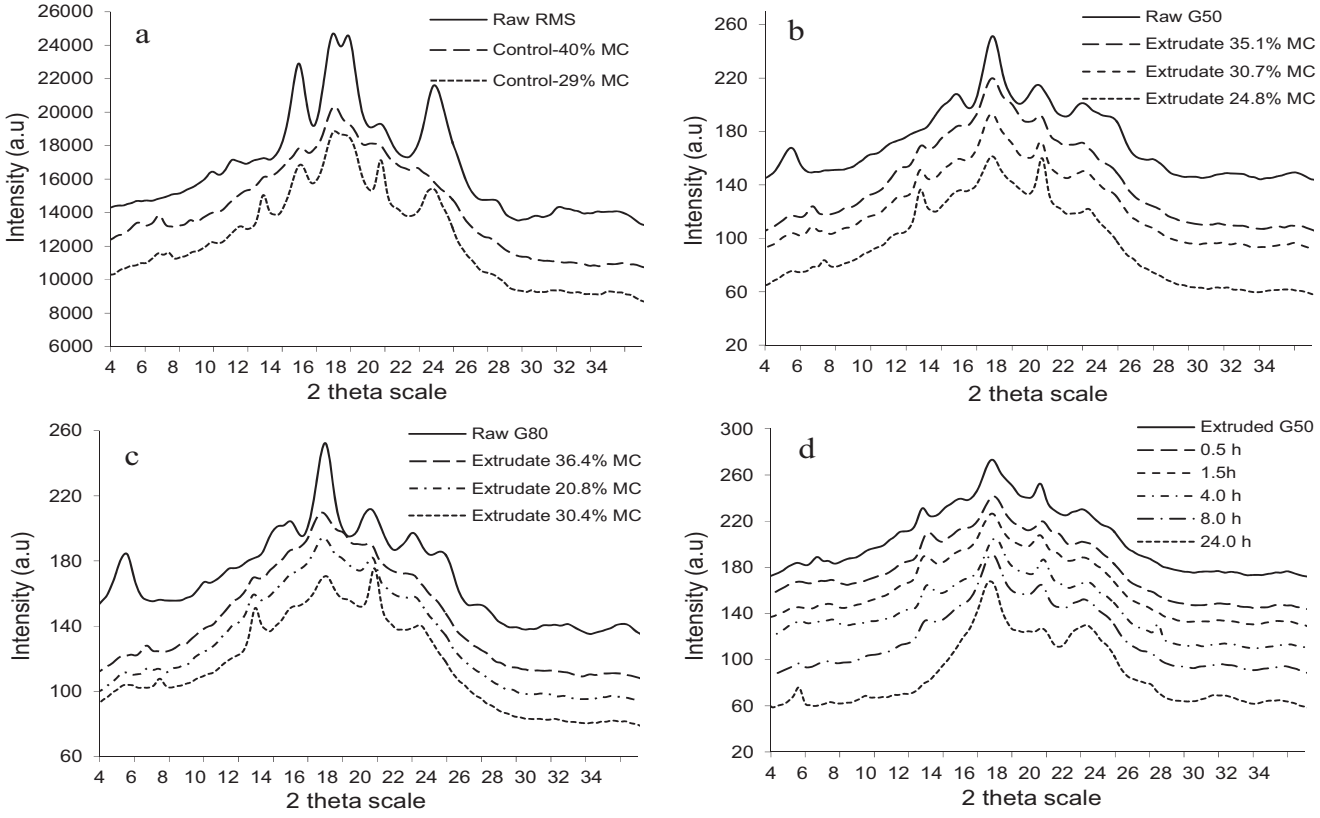

Fig. 2. XRD patterns of raw and extruded (a) RMS, (b) Gelose 50 (G50), (c) Gelose 80 (G80), and (d) extruded and digested G50 at various incubation times. Curves are offset for clarity.

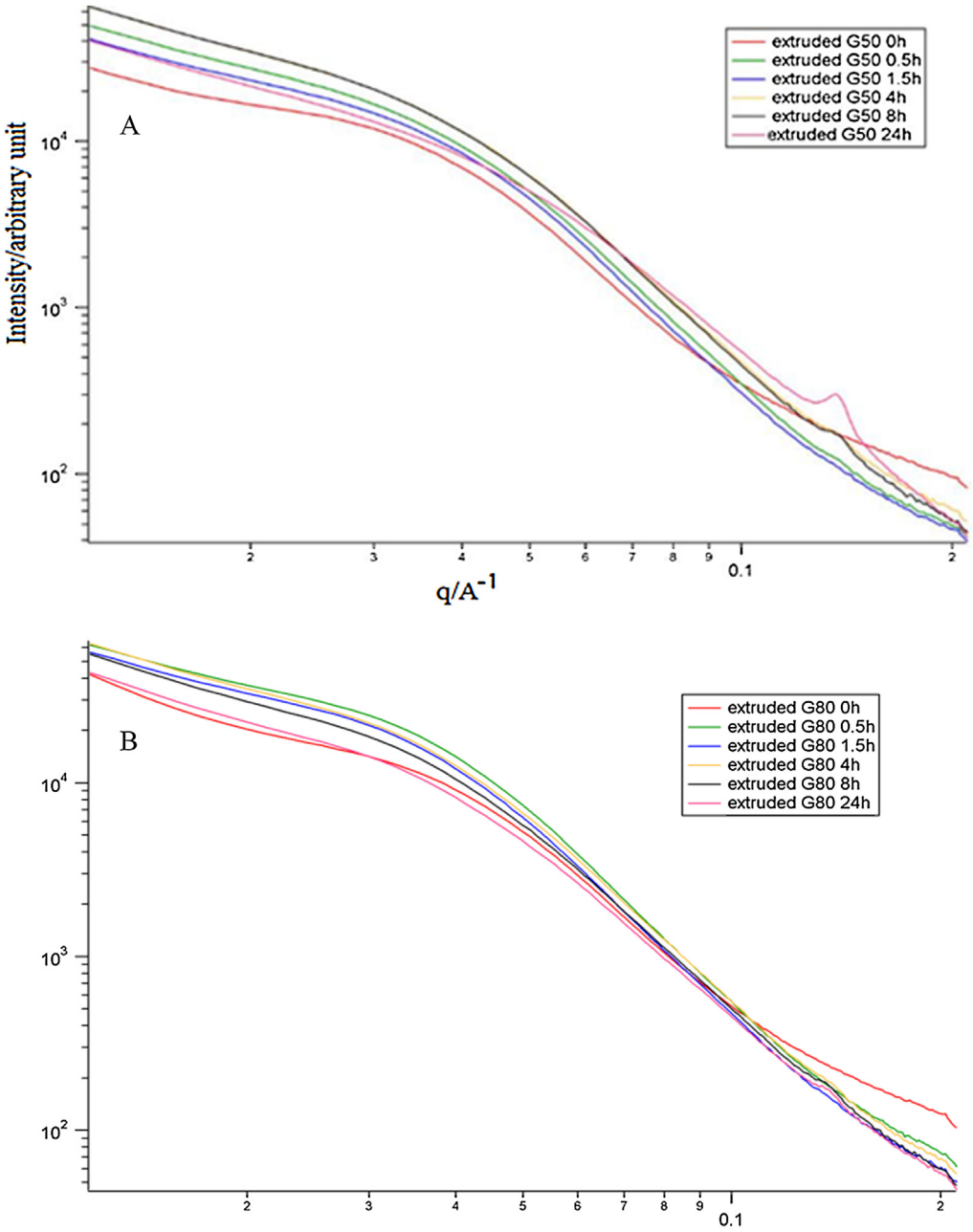

Fig. 3. Small angle X-ray scattering (SAXS) curves of residues of extruded starch G50 (A) and G80 (B) before (0 h) and after digestion for 0 h, 0.5 h, 1.5 h, 4 h, 8 h, and 24 h.

lamellar repeat from starch granules (Blazek & Gilbert, 2011; Lopez-Rubio, Flanagan, Gilbert et al., 2008), but there is still evidence for residual structure. A broad feature at around 0.03 A^{-1} suggests the presence of a motif on the scale of ca. 20 nm for high amylose starches, but to a lesser extent for RMS (data not shown). The appearance of a feature at 0.135 A^{-1} (corresponding to a Bragg distance of ca 4.6 nm) is of more potential relevance to enzyme resistance as it only appears after 4 h of digestion and increases in intensity with subsequent enzyme digestion, particularly for G50 (Fig. 3). This feature has been reported previously for enzyme resistant fractions from high amylose maize starch (Lopez-Rubio, Htoon, & Gilbert, 2007, Zabar, Shimoni, & Bianco-Peled, 2008). It is possible that this feature is connected to the marked increase in double helix and (to a lesser extent) crystallinity with digestion time (Table 3). We also note that the assessment of crystallinity as determined by XRD and SAXS may fundamentally differ as XRD probes dimensions primarily associated with inter-helix order whereas SAXS typically measures order along the chains (Blazek & Gilbert, 2010). One possible structural origin is a conserved length of double helix and/or lateral aggregation of helices involved in stabilizing undigested residues against enzyme attack. Based on the structure of B-type double helices, 4.6 nm corresponds to approximately 13 glucan residues along the helix axis or about three double helices orthogonal to the helix axis (Imberty and Perez, 1988).

3.5. Scanning electron microscopy (SEM)

Fig. 4 shows SEM images of extruded RMS, HAMS and their residues after digestion for various incubation times. SEM images of G50 and G80 appeared to be very similar, therefore, only the images of G50 are shown. Extrusion of granular RMS resulted in a number of small chunks of smooth starchy masses (Fig. 4A). No visible granules were observed under SEM. Additionally, no birefringence was observed under polarized light microscopy suggesting

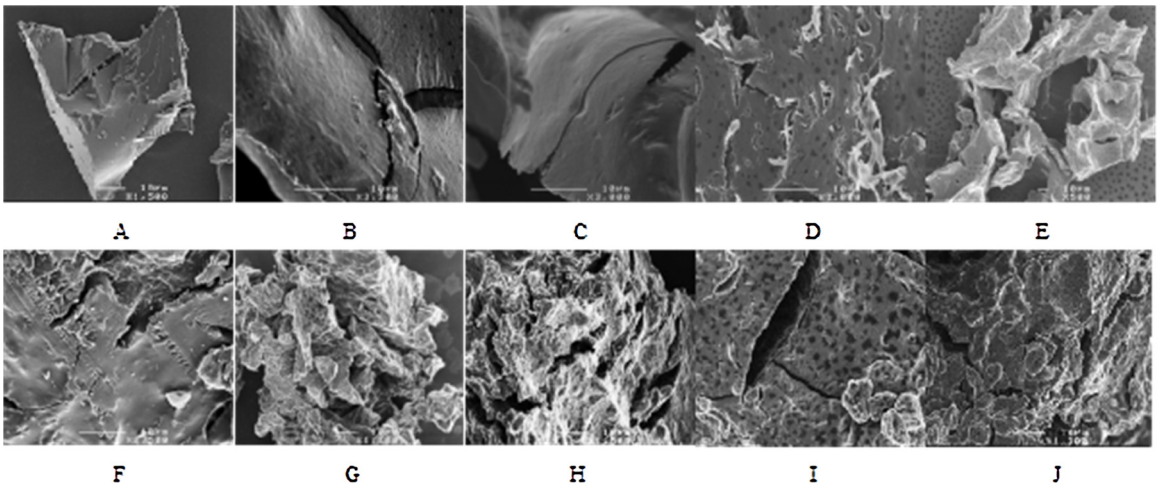

Fig. 4. SEM images of extruded starches and their residues after different digestion times. Upper row: (A) extruded regular maize starch (RMS) and (B)–(E) extruded and digested RMS after 0.5, 1.5, 4 and 8 h incubation, respectively. Lower row: (F) extruded Gelose 50 and (G)–(J) extruded and digested Gelose 50 after 1.5, 4, 8 and 24 h incubation, respectively.

extensive gelatinization (data not shown). Extruded G50 showed a heavily smeared mass containing small fragments embedded in the irregular surface (Fig. 4F). Unlike RMS, both G50 and G80 showed some birefringence with the characteristic Maltese cross pattern, indicating that the current extrusion condition did not completely gelatinize HAMS, a finding also reported previously (Lopez-Rubio, Flanagan, Shrestha et al., 2008; Shrestha et al., 2010).

Residues of digested extruded HAMS and RMS left after 30 min to 24 h digestion times appeared to be different. The digestion pattern of extruded RMS was more homogeneous with the smooth surface slowly eroded by enzyme attack, as shown by apparently random holes (Fig. 4B, 0.5 h and Fig. 4C, 1.5 h). Later stages of digestion seemed to cause fragmentation of the extrudate into smaller pieces (Fig. 4D, 4.0 h) that continued (Fig. 4E, 8.0 h) with longer digestion times.

For extruded G50, initial digestion (Fig. 4G, 1.5 h) did not show any apparent change, but with further digestion (Fig. 4H, 4.0 h) the compact and smeared extrudates appeared to be eroded by amylolysis, as evident by surface holes similar to those observed for extruded RMS (Fig. 4D). Further incubation (Fig. 4I, 8.0 h) made bigger holes and wider gaps in the extruded mass. Further digestion resulted in increased pore numbers and enlarged gaps on the surface of extrudate particles that eventually led to the formation of a number of craters on the extrudate surface (Fig. 4J, 24.0 h).

4. Discussion

4.1. Enzyme digestion of extruded and granular starches is qualitatively different

The enzymic digestion of granular starches under conditions similar to those used here results in residual material in which there is a nearly invariant level of crystallinity during the digestion process for regular maize starch (Zhang and Hamaker 2006; Shrestha et al., 2012) and HAMS (Shrestha et al., 2012). Furthermore, for the three starches studied here, partial digestion of granules led to no major changes in debranched chain length distribution, apart from the more rapid hydrolysis of long chains (DP > 36) in the early stages of digestion for granules of RMS and G50 (Shrestha et al., 2012). This latter effect is comparable with the reduction in the relative proportion of chains of DP > 36 following extrusion (Table 2), consistent with an exposed and load-bearing role for inter-cluster chains within the granular structure. For extruded regular maize starch, this study has also found no marked differences in debranched chain length distributions in material recovered during the digestion process. In contrast, marked changes in debranched chain length distribution are found for extruded G50 and G80 during the digestion process (Fig. 1), with a progressive reduction of chains of DP > 13 for G50 and between DP10 and DP30 for G80, and corresponding increases in short branches (DP < 10). Thus the selectivity of amylase towards local molecular structures in these starches is different between granular and extruded forms whereas no such difference is seen for RMS (Fig. 1; Shrestha et al., 2012). On their own, however, residual branch length distributions are not indicative of enzyme resistance, as both the most susceptible (granular and extruded RMS) and the least susceptible (granular G50 and G80) samples show nearly invariant branch length distributions during digestion, whereas the two samples with intermediate enzyme resistance (extruded G50 and G80) showed the greatest branch length variation during digestion (Fig. 1; Shrestha et al., 2012).

A second qualitative difference in mechanism between enzyme digestion of granular compared with extruded starches is at the mesoscopic level of crystallinity and local polymer organization. For granular starches, apart from a small increase in V-type crystallinity for RMS and B-type crystallinity for the two HAMS, there was no change in mesoscopic order during the process of digestion (Shrestha et al., 2012). This contrasts with the findings of this study which showed major increases in the proportion of crystallinity for all three starches during digestion (Table 3). The increase in crystallinity for RMS and double helix content for G80 over digestion times of 0.5 and 1.5 h and for G50 between 8 and 24 h, were too great to be caused by selective digestion of non-ordered material, so some re-ordering (re-crystallization) must have occurred at least over these time periods. In addition, SAXS data showed the development of a feature corresponding to a Bragg distance of ca. 4.6 nm after prolonged digestion of G50 (Fig. 3) and, to a lesser extent, G80. This feature was not observed after extensive enzyme digestion of granular forms of G50 or G80, but was observed for granular RMS (Shrestha et al., 2012).

A further difference between granular and extruded starches was in the relative extents of double helical order (by NMR) and associated A- or B-type crystallinity (by XRD). Before and during digestion of granular starches, the relative amounts of these two parameters were similar, suggesting that most double helices were part of crystallites. However, after extensive digestion treatment in the present study, both extruded G50 and extruded G80 had much higher measured levels of double helices than crystallinity

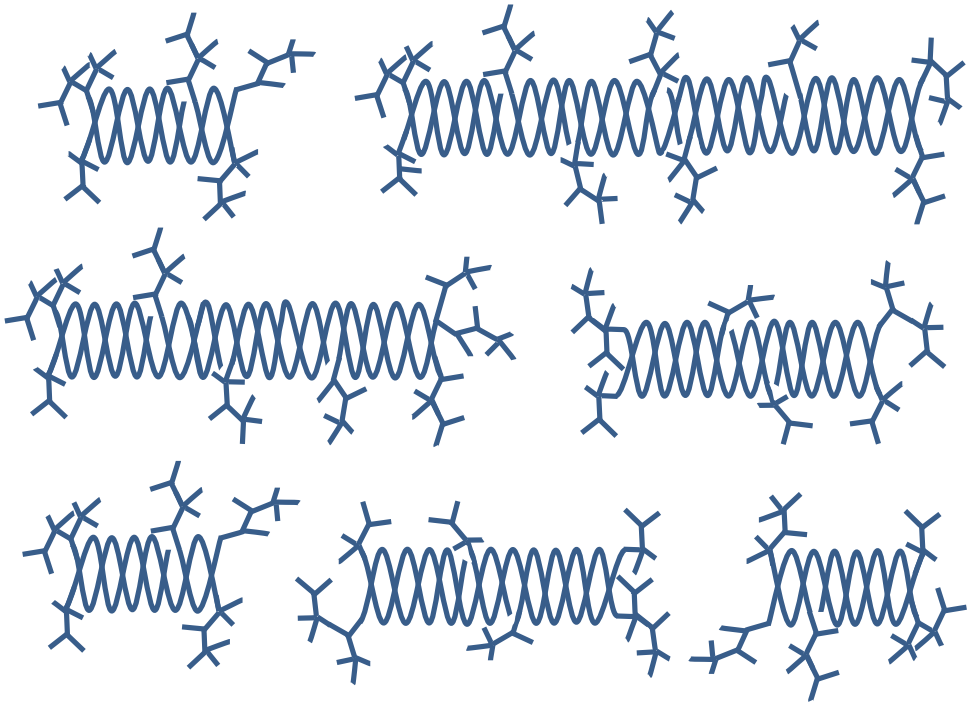

Fig. 5. Model for structure of solid material resistant to long-time enzyme digestion of extruded high amylose starches. An insoluble structure is maintained by a high level of helical order (e.g. ca 70% after 24 h digestion of extruded G50), and enzyme resistance is contributed to by covalently attached highly branched segments (e.g. ca 30% after 24 h digestion of extruded G50) originating from clusters of branch points. A SAXS feature corresponding to a Bragg distance of 4.6 nm may originate from limited aggregation of double helices (diameter ca 1 nm) with attached branch clusters.

(Table 3). For example after 24 h digestion, the extruded G50 residue contained 62% double helix but only 27% crystallinity, and the G80 residue contained 57% double helix and 29% crystallinity. This suggests that many of the double helices that are either resistant from the start of digestion or formed during the digestion process are arranged in a relatively non-crystalline fashion, and yet are resistant to digestion.

These points of distinction between the digestion mechanism of granular and extruded starches lead to the conclusion that the primary digestion-limiting features in granules are microscopic (Blazek & Gilbert, 2010; Shrestha et al., 2012), whereas after extrusion the digestion-limiting features are at the molecular and/or mesoscopic length scales. This is consistent with the presence of a relatively enzyme-resistant surface layer of high amylose maize starches protecting less organized starch chains in the interior of the granule, particularly around the (multiple) hila present in high amylose maize granules (Jiang et al., 2010; Shrestha et al., 2012). Extrusion disrupts this outer layer and exposes the more enzyme-susceptible interior regions to enzyme attack.

4.2. A model for enzyme-resistant structures in extruded high amylose maize starches

The structural features of enzyme-resistant residues after 24 h digestion of G50 or G80 HAMS include a high level of molecular order (Table 3; G50 71%, G80 66%), a modest level of crystallinity (Table 3: G50 29%, G80 31%), structure formation at the 4–5 nm length scale from SAXS (Fig. 3), and branch chain length distributions in which around 30% of chains are of DP 10 or less (Fig. 1). Thus enzyme resistance is accompanied by a simultaneous increase in helix content as well as of short branches which are not considered long enough to form stable helices. We note that these enzyme-resistant structures are not simply due to residual non-gelatinised granules following extrusion, as this would not lead to the marked increase in short branch lengths associated with long-time enzyme resistant solid material (Shrestha et al., 2012). As an approximation, the data from this study suggests that the enzyme-resistant material consists of a combination of (very) short non-ordered branches and longer stretches of glucan chains which can form double helices (and some single helices). The broad spread of debranched chain lengths (Fig. 1) suggests that helices will cover a range of lengths, so the regular repeat distance of ca 4–5 nm from SAXS seems unlikely to be due to very regular short lengths of helix, but may instead reflect a limited but consistent lateral aggregation of helices which gives rise to levels of crystallinity which are much lower than levels of helical order (Table 3). We suggest that this structure (Fig. 5) is a variant on the fringed micelle model proposed by Jane and Robyt (1984), in which residual clusters of branch points coat the surface of (mostly) double helices, thereby limiting lateral aggregation. The enzyme resistance of this structure would be due to a combination of topological restriction of enzyme access to highly branched clusters of branch points which may also provide a physical barrier to the approach of enzymes to inherently slow digestible helices. Densely branched starch polymers are typically water soluble providing facile access of amylase, whereas in the proposed structure these features are associated with a solid particle, thereby providing a greater barrier to enzyme binding. The proposed structural features (Fig. 5) therefore contains two characteristics known to slow down enzyme action (dense branching and double helices) with mutual reinforcement of the enzyme resistance of each. It is also noteworthy that, with increasing enzyme digestion, the proportion of short branches increases for both extruded G50 and G80 (Fig. 1); this suggests that the densely branched structural features are more resistant than the (linear) helical regions. Although the model proposed requires more experimental testing, it is interesting to note that the non-amylopectin fraction in RMS is a classic long chain infrequently-branched amylose, whereas high amylose lines like G50 and G80 contain non-amylopectin fractions with significant branching (Klucinec & Thompson, 1998; Shi, Capitani, Trzasko, & Jeffcoat, 1998). If the proposed structure is correct, it suggests

that the branched amylose-like fractions which are characteristic of high amylose cereal starches may be more efficient in resisting enzyme digestion than purely linear amylose.

Acknowledgements

This work was supported in part by the Australian Research Council (Discovery Grant DP130102461). We acknowledge the facilities, and the scientific and technical assistance of the Australian Microscopy & Microanalysis Research Facility at the Centre for Microscopy and Microanalysis, and the NMR facilities at the Centre for Advanced Imaging at The University of Queensland.

References

Ao, Z., Quezada-Calvillo, R., Sim, L., Nichols, B. L., Rose, D. R., Sterchi, E. E., et al. (2007). Evidence of native starch degradation with human small intestinal maltase-glucoamylase (recombinant). *FEBS Letters*, *581*, 2381–2388.

Bello-Perez, L. A., Ottenhof, M. A., Agama-Acevedo, E., & Farhat, I. A. (2005). Effect of storage time on the retrogradation of banana starch extrudate. *Journal of Agriculture and Food Chemistry*, *53*, 1081–1086.

Bhattacharya, S., & Choudhury, G. G. (1994). Twin-screw extrusion of rice flour: Effect of extruder length-to-diameter ratio and barrel temperature on extrusion parameters and product characteristics. *Journal of Food Process Preservation*, *18*, 389–406.

Bird, A. R., Lopez-Rubio, A., Shrestha, A. K., & Gidley, M. J. (2009). Resistant starch *in vitro* and *in vivo*: Factors determining yield, structure, and physiological relevance. In S. Kasapis, I. T. Norton, & J. B. Ubbink (Eds.), *Modern biopolymer sciences* (pp. 449–512). London: Academic Press.

Bird, A. R., Vuaran, M., Brown, I., & Topping, D. L. (2007). Two high-amylose maize starches with different amounts of resistant starch vary in their effects on fermentation, tissue and digesta mass accretion, and bacterial populations in the large bowel of pigs. *British Journal of Nutrition*, *97*, 134–144.

Blazek, J., & Gilbert, E. P. (2010). The effect of enzymatic hydrolysis on native starch granule structure. *Biomacromolecules*, *11*, 3275–3289.

Blazek, J., & Gilbert, E. P. (2011). Application of small-angle X-ray and neutron scattering techniques to the characterisation of starch structure: A review. *Carbohydrate Polymers*, *85*.

Cairns, P., Sun, L., Morris, V. J., & Ring, S. G. (1995). Physicochemical studies using amylose as an *in-vitro* model for resistant starch. *Journal of Cereal Science*, *21*, 37–47.

Castro, J. V., Ward, R. M., Gilbert, R. G., & Fitzgerald, M. A. (2005). Measurement of the molecular weight distribution of debranched starch. *Biomacromolecules*, *6*, 2260–2270.

Chanvrier, H., Uthayakumaran, S., Appelqvist, I. A. M., Gidley, M. J., Gilbert, E. P., & López-Rubio, A. (2007). Influence of storage conditions on the structure, thermal behaviour, and formation of enzyme-resistant starch in extruded starches. *Journal of Agriculture and Food Chemistry*, *55*, 9883–9890.

Clarke, J. M., Bird, A. R., Topping, D. L., & Cobiac, L. (2007). Excretion of starch and esterified short chain fatty acids by ileostomy subjects after ingestion of acylated starches. *American Journal of Clinical Nutrition*, *86*, 1146–1151.

Dhital, S., Shrestha, A. K., & Gidley, M. J. (2010). Relationship between granule size and in vitro digestibility of maize and potato starches. *Carbohydrate Polymers*, *82*, 480–488.

Dhital, S., Warren, F. J., Butterworth, P. J., Ellis, P. R., & Gidley, M. J. (2015). Mechanisms of starch digestion by α-amylase – structural basis for kinetic properties. *Critical Reviews in Food Science and Nutrition* (in press).

Doutch, J., Bason, M., Franceshcini, F., James, K., Clowes, D., & Gilbert, E. P. (2012). Structural changes during starch pasting using simultaneous Rapid Visco Analysis and small-angle neutron scattering. *Carbohydrate Polymers*, *88*, 1061–1071.

Eerlingen, R. C., Crombez, M., & Delcour, J. A. (1993). Enzyme resistant starch: I. Quantitative and qualitative influence of incubation time and temperature of autoclaved starch on resistant starch formation. *Cereal Chemistry*, *70*, 339–344.

Eerlingen, R. C., Deceuninck, M., & Delcour, J. A. (1993). Enzyme resistant starch: II. Influence of amylose chain length on resistant starch formation. *Cereal Chemistry*, *70*, 345–350.

Gidley, M. J., Cooke, D., Darke, A. H., Hoffmann, R. A., Russell, A. L., & Greenwell, P. (1995). Molecular order and structure in enzyme-resistant retrograded starch. *Carbohydrate Polymers*, *28*, 23–31.

Hizukuri, S. (1986). Polymodal distribution of the chain lengths of amylopectins, and its significance. *Carbohydrate Research*, *147*, 342–347.

Howlett, J., & Ashwell, M. (2008). Glycemic response and health: Summary of a workshop. *American Journal of Clinical Nutrition*, *87*, 212S–216S.

Htoon, A., Shrestha, A. K., Flanagan, B. M., Lopez-Rubio, A., Bird, A. R., Gilbert, E. P., et al. (2009). Effects of processing high amylose maize starches under controlled conditions on structural organization and amylase digestibility. *Carbohydrate Polymers*, *75*, 236–245.

Jane, J., & Robyt, J. F. (1984). Structure studies of amyloe-V complexes and retrograded amylose by action of alpha-amylases, and a new method for preparing amylodextrins. *Carbohydrate Research*, *132*, 105–118.

Jiang, H., Horner, H. T., Pepper, T. M., Blanco, M., Campbell, M., & Jane, J. (2010). Formation of elongated starch granules in high-amylose maize. *Carbohydrate Polymers*, *80*, 533–538.

Kingman, S. M., & Englyst, H. N. (1994). The influence of food preparation methods on the *in vitro* digestibility of starch in potatoes. *Food Chemistry*, *49*, 181–186.

Klucinec, J. D., & Thompson, D. B. (1998). Fractionation of high-amylose maize starches by differential alcohol precipitation and chromatography of the fractions. *Cereal Chemistry*, *75*, 887–896.

Imberty, A., & Perez, S. (1988). A re-visit to the three dimensional structure of B-type starch. *Biopolymers*, *27*, 1205–1221.

Lopez-Rubio, A., Htoon, A., & Gilbert, E. P. (2007). Influence of extrusion and digestion on the nanostructure of high-amylose maize starch. *Biomacromolecules*, *8*, 1564–1572.

Lopez-Rubio, A., Flanagan, B. M., Gilbert, E. P., & Gidley, M. J. (2008). A novel approach for calculating starch crystallinity and its correlation with double helix content: A combined XRD and NMR study. *Biopolymers*, *89*, 761–768.

Lopez-Rubio, A., Flanagan, B. M., Shrestha, A. K., Gidley, M. J., & Gilbert, E. P. (2008). Molecular rearrangement of starch during in-vitro digestion: Towards a better understanding of enzyme resistant starch formation. *Biomacromolecules*, *9*, 1951–1958.

Morell, M. K., Samuel, M. S., & O'Shea, M. G. (1998). Analysis of starch structure using fluorophore-assisted carbohydrate electrophoresis. *Electrophoresis*, *19*, 2603–2611.

O'Shea, M. G., Samuel, M. S., Konik, C. M., & Morell, M. K. (1998). Fluorophore assisted carbohydrate electrophoresis (FACE) of oligosaccharides: Efficiency of labelling and high-resolution separation. *Carbohydrate Research*, *307*, 1–12.

Planchot, V., Colonna, P., & Buleon, A. (1997). Enzymatic hydrolysis of alpha-glucan crystallites. *Carbohydrate Research*, *298*, 319–326.

Shi, Y. C., Capitani, T., Trzasko, P., & Jeffcoat, R. (1998). Molecular structure of a low amylopectin starch and other high amylose maize starches. *Journal of Cereal Science*, *27*, 289–299.

Shrestha, A. K., Ng, C. S., Lopez-Rubio, A., Blazek, J., Gilbert, E. P., & Gidley, M. J. (2010). Enzymatic resistance and structural organization in extruded high amylose maize starch. *Carbohydrate Polymers*, *80*, 699–710.

Shrestha, A. K., Blazek, J., Flanagan, B. M., Dhital, S., Larroque, O., Morell, M. K., et al. (2012). Molecular, mesoscopic and microscopic structure evolution during amylase digestion of maize starch granules. *Carbohydrate Polymers*, *90*, 23–33.

Sievert, D., & Pomeranz, Y. (1989). Enzyme-resistant resistant. I. Characterization and evaluation of enzymatic, thermoanalytical and microscopic methods. *Cereal Chemistry*, *66*, 342–347.

Sievert, D., Czuchajowska, Z., & Pomeranz, Y. (1991). Enzyme-resistant starch: III. X-ray diffraction of autoclaved amylomaize VII starch and enzyme-resistant starch residues. *Cereal Chemistry*, *68*, 86–91.

Siljerstrom, M., Eliasson, A. C., & Bjorck, I. (1989). Characterization of resistant starch from autoclaved wheat starch. *Starch/Starke*, *41*, 147–151.

Tan, I., Flanagan, B., Halley, P. J., Whittaker, A. K., & Gidley, M. J. (2007). A method for estimating the nature and relative proportions of amorphous, single and double helical components in starch granules by C-13 CP/MAS NMR. *Biomacromolecules*, *8*, 885–891.

Topping, D. L., & Clifton, P. (2001). Short chain fatty acids and human colonic function–roles of resistant starch and non starch polysaccharides. *Physiological Reviews*, *81*, 1031–1064.

Wang, J., Yu, L., Xie, F., Chen, L., Li, X., & Liu, H. (2010). Rheological properties and phase transition of cornstarches with different amylose/amylopectin ratios under shear stress. *Starch/Starke*, *62*, 667–675.

Williamson, G., Belshaw, N. J., Self, D. J., Noel, T. R., Ring, S. G., Cairns, P., et al. (1992). Hydrolysis of α-type and β-type crystalline polymorphs of starch by alpha-amylase, beta-amylase and glucoamylase-1. *Carbohydrate Polymers*, *18*, 179–187.

Witt, T., Gidley, M. J., & Gilbert, R. G. (2010). Starch digestion mechanistic information from the time evolution of molecular size distribution. *Journal of Agricultural and Food Chemistry*, *58*, 8444–8452.

Zabar, S., Shimoni, E., & Bianco-Peled, H. (2008). Development of nanostructure in resistant starch type III during thermal treatments and cycling. *Macromolecular Bioscience*, *8*, 163–170.

Zhang, G., & Hamaker, B. R. (2010). Cereal carbohydrates and colon health. *Cereal Chemistry*, *81*, 331–341.

Zhang, G., Ao, Z., & Hamaker, B. R. (2006). Slow digestion property of native cereal starches. *Biomacromolecules*, *7*, 3252–3258.

Zhang, G., Zihua, A. O., & Hamaker, B. R. (2008). Nutritional property of endosperm starches from maize mutants: A parabolic relationship between slowly digestible starch and amylopectin fine structure. *Journal of Agricultural & Food Chemistry*, *56*, 4686–4694.